Radiative decay rates in Si crystallites with a donor ion

Natalia V. Derbenyova and Vladimir A. Burdov[a)]
Lobachevsky State University of Nizhny Novgorod, 23 Gagarin Avenue, 603950 Nizhny Novgorod, Russian Federation

(Received 31 October 2017; accepted 31 January 2018; published online 16 February 2018)

Within the framework of the time-dependent density functional theory, the radiative recombination rates have been calculated for small, ∼1 nm in diameter, hydrogen-passivated silicon crystallites with a single lithium or phosphorus ion. Sharp increase of the radiative recombination rates with increasing temperature was revealed for the crystallites with the lithium ion. No temperature effect was found for the crystallites with the ion of P. It was also shown that the presence of ionized donors in Si crystallites can substantially accelerate the radiative decay compared to the case of pure crystallites. *Published by AIP Publishing*. https://doi.org/10.1063/1.5011382

I. INTRODUCTION

Doping is traditionally used as a means of controllable modification of physical and chemical properties of bulk semiconductors, in particular, bulk silicon. In silicon crystallites, doping is often considered as an efficient method for the improvement of their optical properties. Introduction of shallow impurities can strongly modify the electronic structure of Si crystallites[1–6] and, as a consequence, influence the electron-hole radiative transitions.

There are lots of contradictory experimental data about the influence of impurities on the luminescent properties of Si crystallites. Among them, reports on the enhancement (within an order of magnitude) of the photoluminescence intensity often appear, especially for 2–10 nm in the diameter crystallites with phosphorus or with phosphorus and boron.[6–13] Theoretical study of P-doped, or B&P-codoped, Si crystallites has been also carried out earlier. In particular, electronic structure and formation energy,[14–17] as well as optical absorption spectra,[18–20] have been calculated using first-principle methods. Radiative recombination rates were computed in P-doped Si crystallites with diameters greater than 2 nm, and their increase caused by the P doping was predicted as a result of the efficient Γ-*X* mixing.[10,21] It is possible to expect, however, that crystallites with smaller sizes, especially ∼1 nm in diameter or less, will demonstrate faster radiative transitions, as follows from the calculations of Ramos *et al.*[22] performed for Si crystallites at room temperature. Therefore, it is interesting to estimate the values and trace the temperature dependence of the radiative decay rates for such small Si crystallites with phosphorus.

Si crystallites with Li were essentially less studied. The photoluminescence spectra were measured,[23] and blue shift of the photoluminescence peak and some decrease of the radiative lifetime were observed in Si crystallites after their doping with lithium. Also, formation energies were calculated earlier for the Li-doped Si crystallites.[24] These calculations have shown that the central location for Li (as well as for P) is more preferable energetically. Theoretical treatment of the optical properties of Li-doped crystallites is, in fact, absent at present.

In respect of the crystallites with impurities, the following principal question arises: is introduction of impurities (in particular, donors, in our case) capable of accelerating the radiative interband transitions? In order to answer this question, we have to calculate the radiative decay rates for the Si crystallites with donors. In the present paper, within the framework of *ab initio* methods, we calculate the radiative recombination rates in small silicon crystallites (∼1 nm in diameter) with Li and P: $Si_{34}H_{36}P$; $Si_{30}H_{40}Li$; $Si_{46}H_{60}P$; and $Si_{42}H_{64}Li$. Following Chan *et al.*,[24] we also assume the central position of the donor inside the crystallite to be more preferable from the energy point of view. Therefore, only Si crystallites with centrally located donors are considered below. Initially, the decay rates of the basic electron-hole radiative transitions are computed between the lowest unoccupied molecular orbital (LUMO) and the highest occupied molecular orbital (HOMO). In the following, however, we take into account also excited electron-hole states which may contribute to the luminescence with high efficiency at finite temperature. Consequently, the rates of the radiative decay become temperature-dependent.

The presence of a donor inside a crystallite can affect the luminescent kinetics in two ways. First, the electric field of the donor ion modifies the electron wave functions and, consequently, the matrix elements and the probabilities of the radiative interband transitions. Second, the donor atom is a source of an extra electron which makes the Auger recombination unavoidable after the excitation of an electron-hole pair inside the crystallite. Nevertheless, as has been already mentioned, a significant enhancement of the photoluminescence is often observed in Si crystallites after their doping with phosphorus. This allows us to suppose that the Auger process is strongly suppressed, and the radiative channel is not "shunted" by the nonradiative one. Perhaps, the extra electron (emitted by the donor after its introduction into the crystallite) leaves the crystallite and occupies some deep center somewhere near the crystallite. Since experimental observations of photoluminescence in real crystallites are always separated in time with the process of their formation, we may assume that the excessive electron has enough time to "find" such a deep center while the process of photo-excitation does

[a)]Authors to whom correspondence should be addressed: vab3691@yahoo.com

not start. Consequently, the donor inside the crystallite turns into an ion and remains uncompensated during the processes of the crystallite excitation and subsequent photon emission. Obviously, in this case, the Auger recombination will be, indeed, suppressed. In our subsequent calculations, we suppose that the emitted electron is captured by some deep center outside the crystallite and consider Li and P as positive ions but not as neutral atoms.

II. METHOD OF CALCULATION

The silicon crystallites are constructed from the bulk Si lattice by cutting a sphere centered with respect to an atom or a tetrahedral interstitial. All dangling bonds are saturated by hydrogen. The obtained crystallites are relaxed with the Avogadro code[25] using the universal force field method.[26] Further correction of the structure is performed with the algorithm Basin Hopping[27,28] using the BFGS method[29] based on the density functional theory (DFT), which is realized in the Octopus package[30] combined with the Atomic Simulation Environment (ASE).[31] The relaxation procedure continues until maximum (over the crystallite) Hellmann-Feynman forces become less than 10^{-4} eV/Å. At the next step, the P or Li ion is introduced into the center of the relaxed crystallite (instead of the Si atom or into the interstitial, respectively), and the above described optimization procedure is repeated.

Two pairs of the optimized crystallites with Li^+ (upper row) and P^+ (lower row) (in the following we shall denote the ions simply as Li and P) are presented in Fig. 1. Because of small number of atoms, all the crystallites have the shape that is not exactly spherical. In order to characterize the crystallite size, we introduce a mean radius for each crystallite as a mean distance from the donor ion to the surface hydrogen atoms.[32] Radii of the optimized crystallites $Si_{30}H_{40}Li$, $Si_{42}H_{64}Li$, $Si_{34}H_{36}P$, and $Si_{46}H_{60}P$ equal 5.28, 5.98, 5.53, and 6.17 Å, respectively.

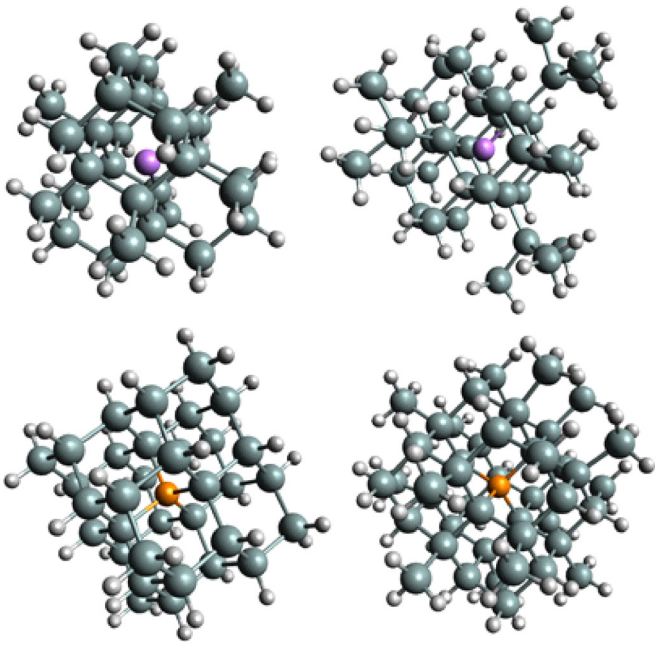

FIG. 1. $Si_{30}H_{40}Li$ (upper left) and $Si_{42}H_{64}Li$ (upper right) crystallites, and $Si_{34}H_{36}P$ (lower left) and $Si_{46}H_{60}P$ (lower right) crystallites. Big balls represent the Si atoms, small balls represent the H atoms, and the central ball represents the Li or P ion.

After the geometry was optimized, the electronic structure of Si crystallites was determined by the DFT method employing the Octopus package[30] in which the Kohn-Sham equations[33] are solved on a grid with the use of pseudopotentials. Optimal values of the grid spacing and the supercell size were selected under the requirement that the change of the total crystallite energy be less than 0.01 eV when varying these parameters. As the boundary condition, we set the wave function to be zero at the supercell surface. The generalized gradient approximation (GGA-PBE)[34] was used for the exchange-correlation functional. To exclude electron self-interaction, the Perdew-Zunger correction[35] has been taken into account.

As known, the DFT has principle difficulties with a description of excited states of many-electron systems. Therefore, in order to correctly describe single-particle excitations of the electron subsystem of the Si crystallites, we then apply time-dependent density functional theory (TD DFT) in the Casida's formulation[36] developed specifically for finite-size systems. This method will allow us to calculate the excitations' energies and the optical matrix elements in a self-consistent manner. The TD DFT single-particle wave functions are obtained as linear combinations of the Kohn-Sham orbitals.

III. DENSITY OF EXCITED STATES (DOES)

First of all, within the framework of the TD DFT, we compute the spectra of the single-particle excitations in the Si crystallites with the phosphorus and lithium ions and determine the density of states for these excitations, which is referred to in the following as the density of excited states (DOES). Figure 2 demonstrates calculated DOES within the energy window of 0.1 eV ($\sim 4k_BT$ at room temperature) above the HOMO-LUMO gap ε_g. It is seen that in the crystallites with Li the excitations' spectra have substantially higher density than in the crystallites with P: there are many DOES peaks inside the chosen energy window, and most of them are non-degenerate (the peaks are so normalized that the values of their maxima equal the number of states at the

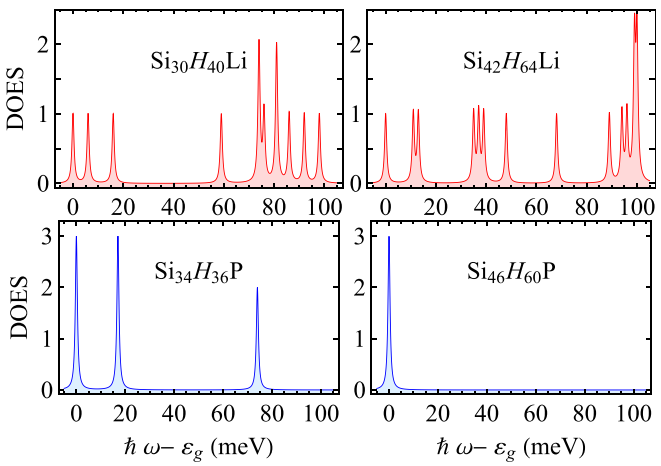

FIG. 2. Density of excited states for Si crystallites with Li and P ions.

corresponding energies), while in the crystallites with P, only three (for $Si_{34}H_{36}P$) or, even, one (for $Si_{46}H_{60}P$) DOES peak with triple and double degeneracies exist inside the window.

According to the tetrahedral symmetry of the system, and due to the valley-orbit interaction[37] caused by the short-range potential[38] of the donor ion, the LUMO-state splits into singlet, doublet, and triplet. Both crystallites with Li have the so-called inverse level structure that is typical for the bulk Si:[39] the singlet level lies higher than the doublet and triplet ones. As the DFT calculations show, in $Si_{30}H_{40}Li$ crystallite, the triplet is the ground state, while in $Si_{42}H_{64}Li$ crystallite, it is the doublet. The crystallites with P have the standard structure of the level splitting with the singlet being the ground conduction state and the triplet being the first excited state. The singlet-triplet splitting is strengthened in crystallites by a quantum confinement. Its value equals several tenths of eV in the crystallites with P, while in the crystallites with Li typical energies of the singlet-doublet-triplet splitting are several times less. The HOMO-state remains triply degenerate in accordance with the tetrahedral symmetry of the structure independently of the ion existence in the crystallite.

Validity of this picture, however, is not absolute. The TD DFT method allows one to obtain more precise data showing that the degeneracy is almost completely removed in Si crystallites with the Li ion except for two doubly degenerate energies in each crystallite. On the contrary, the crystallites with the P ion conserve the degeneracies of the energy levels obtained within the standard DFT. We have revealed that the insertion of lithium leads to the considerably stronger Jahn-Teller distortions of the lattice than that of phosphorus. We can compare, for instance, two close in sizes crystallites: $Si_{34}H_{36}P$ and $Si_{30}H_{40}Li$. Both Li and P ions have four Si nearest neighbours. After the geometry optimization procedure, the distances r_j $(j = 1, 2, 3, 4)$ from the donor ion to its four neighbours become different. An estimation of the standard deviation calculated as the square root of $\sum_{j=1}^{4}(r_j - \bar{r})^2/4$ for $Si_{34}H_{36}P$ crystallite yields 0.01 Å, while for $Si_{30}H_{40}Li$ crystallite this value turns out to be four times greater. Evidently, in the crystallites with Li, the deviations from the tetrahedral symmetry are sufficient to reduce the degeneracy and split (completely or partially) the energy levels.

It is also interesting to compare electronic states in the crystallites with and without donors. For this purpose, we have plotted in Fig. 3 the DOES for the corresponding pure crystallites being the prototypes for the crystallites considered here with ions. As seen, an introduction of the phosphorus ion leads to a reduction of the DOES—the pure crystallites have more developed structure of excited states (compare with lower panels in Fig. 2). Evidently, this is mainly due to the significant rarefication of the energy levels in the conduction band caused by the valley-orbit interaction accompanied by the strong splitting-off of the singlet level. An introduction of Li acts oppositely: the DOES substantially increases (see upper panels in Fig. 2) compared to the undoped crystallite (upper panels in Fig. 3).

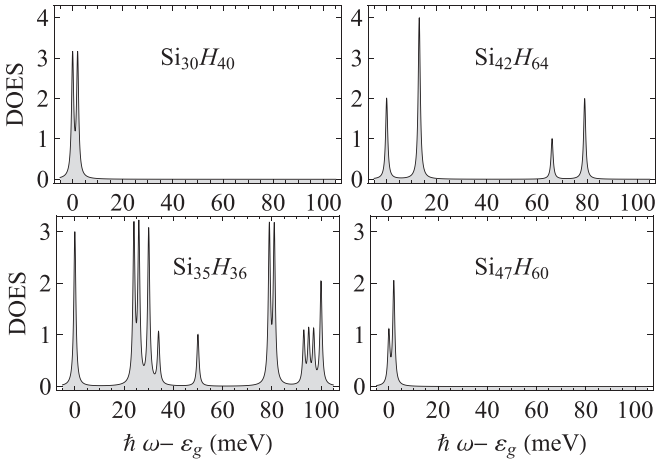

FIG. 3. Density of excited states for the four prototypical pure Si crystallites.

IV. RADIATIVE RECOMBINATION RATES

Radiative relaxation of the single-particle excitations can be characterized by the decay rate obtained with the Fermi golden rule

$$\tau_{if}^{-1} = \frac{2\pi}{\hbar}\sum_{\mathbf{q},\alpha}|W_{if}|^2\delta(\varepsilon_{if} - \hbar\omega_\alpha(\mathbf{q})), \tag{1}$$

for the transition from the initial (some excited) state i to the final (ground) state f of the many-electron subsystem of the crystallite. Here, $\omega_\alpha(\mathbf{q})$ stands for the frequency of the emitted photon with the wave vector $\mathbf{q}$ and polarization α, ε_{if} is the energy of the single-particle excitation, and W_{if} is the matrix element of the operator

$$\hat{W} = \sum_{\mathbf{q}',\lambda}\sqrt{\frac{2\pi\hbar e^2}{m_0^2\omega_\lambda(\mathbf{q}')\epsilon V}}\left(\hat{a}_{\mathbf{q}'\lambda} + \hat{a}^\dagger_{\mathbf{q}'\lambda}\right)\mathbf{e}_{\mathbf{q}'\lambda}\hat{\mathbf{p}}, \tag{2}$$

describing the electron-photon interaction. $\hat{\mathbf{p}}$ is the electron momentum operator, $\mathbf{e}_{\mathbf{q}'\lambda}$ is the polarization vector, the operator $\hat{a}_{\mathbf{q}'\lambda}$ annihilates and $\hat{a}^\dagger_{\mathbf{q}'\lambda}$ creates a photon with the wave vector $\mathbf{q}'$ and polarization λ, V stands for the volume of the electromagnetic resonator that is usually chosen equal to the supercell volume,[18] and ϵ is the permittivity of the crystallite surrounding. When calculating the rates, we set $\epsilon = 4$, which is typical for the SiO_2 matrix.[40] An ensemble of photons is described by the Bose-Einstein statistics. After the transition, the number of photons increases by one.

After some algebra, the recombination rate can be written as

$$\tau_{if}^{-1} = \frac{4e^2\varepsilon_{if}|\mathbf{p}_{if}|^2\sqrt{\epsilon}}{3m_0^2\hbar^2c^3}, \tag{3}$$

where $\mathbf{p}_{if} = \langle\psi_i|\hat{\mathbf{p}}|\psi_f\rangle$ is the momentum matrix element with respect to the initial ψ_i and final ψ_f wave functions computed self-consistently in common with the excitation energy ε_{if} within the TD DFT Casida's approach[36] as has been pointed out above.

Initially, we calculate the decay rates of the HOMO-LUMO transitions, which equal the following: 1.8×10^6 s^{-1}

(in $Si_{34}H_{36}P$ crystallite); 8×10^6 s^{-1} (in $Si_{46}H_{60}P$ crystallite); 6.5×10^4 s^{-1} (in $Si_{30}H_{40}Li$ crystallite); and 7×10^4 s^{-1} (in $Si_{42}H_{64}Li$ crystallite). The rate values in the corresponding pure crystallites are as follows: 10^7 s^{-1} (in $Si_{35}H_{36}$ crystallite); 10^5 s^{-1} (in $Si_{47}H_{60}$ crystallite); 4×10^5 s^{-1} (in $Si_{30}H_{40}$ crystallite); and 3.6×10^6 s^{-1} (in $Si_{42}H_{64}$ crystallite). As seen, the crystallites with the phosphorus ion demonstrate (~2 orders of magnitude) faster radiative HOMO-LUMO transitions than the crystallites with Li. The latter also exhibit slower HOMO-LUMO transitions than the corresponding prototypical pure crystallites. The crystallite $Si_{34}H_{36}P$ has the rate several times lesser than $Si_{35}H_{36}$ crystallite, while the crystallite $Si_{46}H_{60}P$ has the rate ~2 orders of magnitude greater than $Si_{47}H_{60}$ crystallite. Accordingly, the introduction of phosphorus seems to be more preferable for improving the luminescent properties of Si crystallites than the introduction of lithium.

It is worth noting, however, that at finite temperature not only the HOMO-LUMO radiative transition but also the transitions with the energies slightly (within several k_{BT}) greater than the fundamental gap ε_g become possible and can contribute to the luminescence. As a rule, the HOMO-LUMO radiative transition is much slower than the nonradiative transitions (which are due to the interaction with a boson bath of temperature T) between the excited states of the electronic subsystem. These nonradiative transitions provide fast energy exchange between the excited states and their relaxation to the long-living lowest excited state with the HOMO-LUMO radiative transition. In this case, it is possible to introduce some effective radiative rate determined as the statistical average over all excited states with the excitation (electron-hole) energies ε_{if} greater than ε_g,

$$\tau^{-1}(T) = \frac{\sum_f \tau_{if}^{-1} \exp\left[-(\varepsilon_{if} - \varepsilon_g)/k_B T\right]}{\sum_f \exp\left[-(\varepsilon_{if} - \varepsilon_g)/k_B T\right]}, \tag{4}$$

where k_B stands for the Boltzmann constant. The temperature dependencies of the decay rates τ^{-1} calculated according to Eqs. (1), (3), and (4) for the crystallites with Li and P are presented in Fig. 4.

It is seen that the decay rates in the crystallites with Li and P behave quite differently. If in the crystallites with P the rates remain almost invariable, in the crystallites with Li the rates drastically rise by ~3 (for $Si_{42}H_{64}Li$) and ~2 (for $Si_{30}H_{40}Li$) orders of magnitude at room temperature. As a result, being initially (at $T \to 0$) 1–2 orders of magnitude smaller than the rates in the "corresponding" close in size crystallites with the phosphorus ion, at room temperature the decay rates in the crystallites with Li become several times—order of magnitude greater, respectively.

Such a behavior of the decay rates is caused by the electronic structure of the considered crystallites. As shown in Fig. 2, in $Si_{46}H_{60}P$ crystallite, there are no transitions (within the chosen energy window 0.1 eV) giving rise to the luminescence, other than the HOMO-LUMO one. In $Si_{34}H_{36}P$ crystallite, the triply and doubly degenerate additional excited states appear near the lowest state with the HOMO-LUMO transition. However, as the calculations show, the radiative annihilation of these states has vanishing rates. Therefore, their presence results only in the ~ twofold decrease of the statistic weight of the HOMO-LUMO transition. In the crystallites with Li, many excited states exist in the nearest vicinity of the lowest (HOMO-LUMO) state with the annihilation rates much greater than the HOMO-LUMO transition rate. As a result, $\tau^{-1}(T)$ for the crystallites with lithium ion sharply rises as T increases.

Finally, it is interesting to trace an influence of the ion introduction on the radiative decay rates in Si crystallites with increasing temperature. For better visualization, we define here the relative decay rate μ as the ratio

$$\mu = \tau^{-1}(T)/\tau_0^{-1}(T), \tag{5}$$

where $\tau^{-1}(T)$ has a prior meaning and $\tau_0^{-1}(T)$ stands for the effective decay rate [Eq. (4)] for the corresponding Si crystallites without ions. Results of our calculations for the four silicon crystallites considered here are presented in Fig. 5.

As has been already pointed out, the rates of the HOMO-LUMO transitions in the crystallites with Li ion are much less than the ones in the corresponding Li-free prototypes. In fact, only the HOMO-LUMO transitions occur at $T = 0$. Therefore, the rates shown in both Figs. 4 and 5 at zero temperature are precisely the rates of the HOMO-LUMO transitions. As T increases, the decay rates rise not only absolutely but also relatively—with respect to their values in pure crystallites. At room temperature, the values of

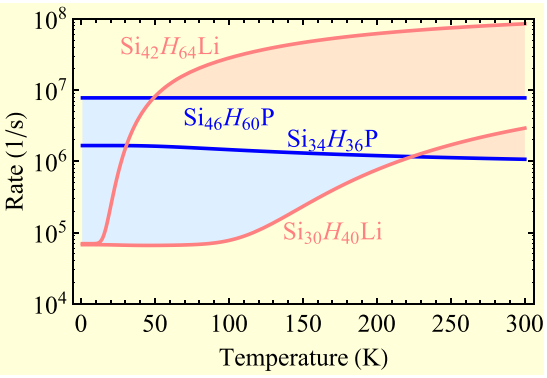

FIG. 4. Temperature dependence of the radiative decay rates for the crystallites with the P and Li ions.

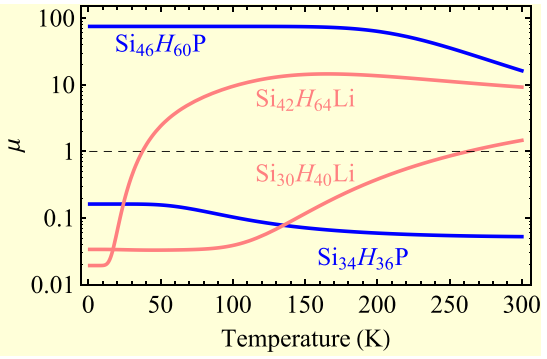

FIG. 5. Temperature dependence of the relative decay rates for the crystallites with the P and Li ions.

the decay rates in the crystallites with Li turn out to be greater than in the pure crystallites. This means that at room temperature, the lithium introduction positively influences the optical properties of Si crystallites. The crystallites with phosphorus exhibit some decrease of the relative decay rate μ with increasing T. Nevertheless, in $Si_{46}H_{60}P$ crystallite, μ always remains much greater than unity, while in $Si_{34}H_{36}P$ crystallite $\mu < 1$ at any temperature.

V. CONCLUSION

Thus, the TD DFT calculations performed here have shown temperature-dependent and independent of temperature radiative decay in the small silicon crystallites with lithium and phosphorus, respectively. The sharp rise of the decay rate in the crystallites with Li at increasing T is caused by the participation of the higher excited states in the radiative transitions with shorter lifetimes and greater (within several k_{BT}) energies. Perhaps, this can explain the observed experimental blue shift of the photoluminescence peak and increase of the photoluminescence rate in silicon crystallites after their doping with lithium.[23] In the crystallites with phosphorus, all the interband transitions, other than the HOMO-LUMO one, are either slow or strongly separated in energy ($\gg k_BT$) from the HOMO-LUMO transition and, therefore, suppressed at any temperatures. As a consequence, the radiative transitions in the crystallites with phosphorus occur with the rates close to the rate of the basic HOMO-LUMO transition.

Our recent investigations[41] show that the greater crystallites (up to 2 nm in diameter) with Li and P behave, on the whole, similarly. In particular, the crystallites with P do not exhibit any temperature dependence on the radiative recombination rates, while some of the crystallites with Li ion demonstrate rising τ^{-1} with increasing T. However, in the greater crystallites with Li, this temperature effect is not so pronounced as in the crystallites considered here.

It should be noted that the exchange interaction, which was not taken here into account, can produce some additional splitting of the exciton energy levels with typical spacings of the order of meV.[42,43] In the absence of impurities, this fine structure of the exciton states also causes a temperature dependence of the radiative recombination rate.[44,45] It seems, however, that the influence of the donor ion is considerably stronger—the typical values of the energy splitting due to the presence of the donor are of the order of 100 meV. Therefore, it is natural to expect that the rate values will not be essentially affected by the exchange interaction, at least, at room temperature. At the same time, some changes of the temperature dependence of the rates at $T \to 0$ are possible.

ACKNOWLEDGMENTS

The work was supported by the Russian Ministry of Education and Science (Assignment No. 3.2637.2017/4.6 and the Project No. RFMEFI61614X0008) and the Russian Foundation for Basic Research (Project No. 16-32-00683). The calculations were performed with the use of the supercomputer complexes "Lobachevsky"[46] and"Lomonosov."[47]

[1]A. Mimura, M. Fujii, S. Hayashi, D. Kovalev, and F. Koch, Phys. Rev. B **62**, 12625 (2000).
[2]G. A. Kachurin, S. G. Cherkova, V. A. Volodin, V. G. Kesler, A. K. Gunakovsky, A. G. Cherkov, A. V. Bublikov, and D. I. Tetelbaum, Nucl. Instrum. Methods B **222**, 497 (2004).
[3]J. R. Chelikowsky, M. M. G. Alemany, T.-L. Chan, and G. M. Dalpian, Rep. Prog. Phys. **74**, 046501 (2011).
[4]B. L. Oliva-Chatelain, T. M. Ticich, and A. R. Barron, Nanoscale **8**, 1733 (2016).
[5]E. Arduca and M. Perego, Mater. Sci. Semicond. Process. **62**, 156 (2017).
[6]K. Nomoto, H. Sugimoto, A. Breen, A. V. Ceguerra, T. Kanno, S. P. Ringer, I. Perez-Wurfl, G. Conibeer, and M. Fujii, J. Phys. Chem. C **120**, 17845 (2016).
[7]M. Fujii, A. Mimura, S. Hayashi, and K. Yamamoto, Appl. Phys. Lett. **75**, 184 (1999).
[8]D. I. Tetelbaum, S. A. Trushin, V. A. Burdov, A. I. Golovanov, D. G. Revin, and D. M. Gaponova, Nucl. Instrum. Methods B **174**, 123 (2001).
[9]A. N. Mikhaylov, D. I. Tetelbaum, V. A. Burdov, O. N. Gorshkov, A. I. Belov, D. A. Kambarov, V. A. Belyakov, V. K. Vasiliev, A. I. Kovalev, and D. M. Gaponova, J. Nanosci. Nanotechnol. **8**, 780 (2008).
[10]V. A. Belyakov, A. I. Belov, A. N. Mikhaylov, D. I. Tetelbaum, and V. A. Burdov, J. Phys.: Condens. Matter **21**, 045803 (2009).
[11]K. Nomoto, T. C.-J. Yang, A. V. Ceguerra, A. Breen, L. Wu, X. Jia, T. Zhang, B. Puthen-Veettil, Z. Lin, S. Ringer, G. Conibeer, and I. Perez-Wurfl, Appl. Phys. Express **9**, 115001 (2016).
[12]K. Nomoto, T. C.-J. Yang, A. V. Ceguerra, T. Zhang, Z. Lin, A. Breen, L. Wu, B. Puthen-Veettil, X. Jia, G. Conibeer, I. Perez-Wurfl, and S. P. Ringer, J. Appl. Phys. **122**, 025102 (2017).
[13]T. C.-J. Yang, K. Nomoto, B. Puthen-Veettil, Z. Lin, L. Wu, T. Zhang, X. Jia, G. Conibeer, and I. Perez-Wurfl, Mater. Res. Express **4**, 075004 (2017).
[14]D. V. Melnikov and J. R. Chelikowsky, Phys. Rev. Lett. **92**, 046802 (2004).
[15]Z. Zhou, M. L. Steigerwald, R. A. Friesner, L. Brus, and M. S. Hybertsen, Phys. Rev. B **71**, 245308 (2005).
[16]Q. Xu, J.-W. Luo, S.-S. Li, J.-B. Xia, J. Li, and S.-H. Wei, Phys. Rev. B **75**, 235304 (2007).
[17]S. Ossicini, E. Degoli, F. Iori, E. Luppi, R. Magri, G. Cantele, F. Trani, and D. Ninno, Appl. Phys. Lett. **87**, 173120 (2005).
[18]F. Iori, E. Degoli, E. Luppi, R. Magri, I. Marri, G. Cantele, D. Ninno, F. Trani, and S. Ossicini, J. Lumin. **121**, 335 (2006).
[19]Z. Ni, X. Pi, S. Cottenier, and D. Yang, Phys. Rev. B **95**, 075307 (2017).
[20]F. Iori, E. Degoli, M. Palummo, and S. Ossicini, Superlattices Microstruct. **44**, 337 (2008).
[21]V. A. Belyakov and V. A. Burdov, Phys. Rev. B **79**, 035302 (2009).
[22]L. E. Ramos, E. Degoli, G. Cantele, S. Ossicini, D. Ninno, J. Furthmüller, and F. Bechstedt, Phys. Rev. B **78**, 235310 (2008).
[23]E. Klimesova, K. Kusova, J. Vacik, V. Holy, and I. Pelant, J. Appl. Phys. **112**, 064322 (2012).
[24]T.-L. Chan, H. Kwak, J.-H. Eom, S. B. Zhang, and J. R. Chelikowsky, Phys. Rev. B **82**, 115421 (2010).
[25]M. D. Hanwell, D. E. Curtis, D. C. Lonie, T. Vandermeersch, E. Zurek, and G. R. Hutchison, J. Cheminf. **4**, 17 (2012).
[26]A. K. Rappe, C. J. Casewit, K. S. Colwell, W. A. Goddard III, and W. M. Skiff, J. Am. Chem. Soc. **114**, 10024 (1992).
[27]D. J. Wales and J. P. K. Doye, J. Phys. Chem. A **101**, 5111 (1997).
[28]D. J. Wales and H. A. Scheraga, Science **285**, 1368 (1999).
[29]R. Fletcher, *Practical Methods of Optimization*, 2nd ed. (John Wiley & Sons, New York, 1987).
[30]A. Castro, H. Appel, M. Oliveira, C. A. Rozzi, X. Andrade, F. Lorenzen, M. A. L. Marques, E. K. U. Gross, and A. Rubio, Phys. Status Solidi B **243**, 2465 (2006).
[31]A. H. Larsen, J. J. Mortensen, J. Blomqvist, I. E. Castelli, R. Christensen, M. Dulak, J. Friis, M. N. Groves, B. Hammer, C. Hargus, E. D. Hermes, P. C. Jennings, P. B. Jensen, J. Kermode, J. R. Kitchin, E. L. Kolsbjerg, J. Kubal, K. Kaasbjerg, S. Lysgaard, J. B. Maronsson, T. Maxson, T. Olsen, L. Pastewka, A. Peterson, C. Rostgaard, J. Schiotz, O. Schutt, M. Strange, K. S. Thygesen, T. Vegge, L. Vilhelmsen, M. Walter, Z. Zeng, and K. W. Jacobsen, J. Phys.: Condens. Matter **29**, 273002 (2017).
[32]L. E. Ramos, E. Degoli, G. Cantele, S. Ossicini, D. Ninno, J. Furthmuller, and F. Bechstedt, J. Phys.: Condens. Matter **19**, 466211 (2007).
[33]W. Kohn and L. J. Sham, Phys. Rev. **140**, A1133 (1965).
[34]J. P. Perdew, K. Burke, and M. Ernzerhof, Phys. Rev. Lett. **77**, 3865 (1996).
[35]J. P. Perdew and A. Zunger, Phys. Rev. B **23**, 5048 (1981).

[36]M. E. Casida, in *Recent Developments and Applications of Modern Density Functional Theory*, edited by J. M. Seminario (Elsevier Science, Amsterdam, 1996), p. 391.
[37]W. Kohn and J. M. Luttinger, Phys. Rev. **97**, 1721 (1955).
[38]S. T. Pantelides and C. T. Sah, Phys. Rev. B **10**, 621 (1974).
[39]R. A. Faulkner, Phys. Rev. **184**, 713 (1969).
[40]J. D. Casperson, L. D. Bell, and H. A. Atwater, J. Appl. Phys. **92**, 261 (2002).
[41]N. V. Derbenyova and V. A. Burdov, J. Phys. Chem. C **122**, 850 (2018).
[42]F. A. Reboredo, A. Franceschetti, and A. Zunger, Appl. Phys. Lett. **75**, 2972 (1999).
[43]F. A. Reboredo, A. Franceschetti, and A. Zunger, Phys. Rev. B **61**, 13073 (2000).
[44]P. D. J. Calcott, K. J. Nash, L. T. Canham, M. J. Kane, and D. Brumhead, J. Phys.: Condens. Matter **5**, L91 (1993).
[45]P. D. J. Calcott, K. J. Nash, L. T. Canham, M. J. Kane, and D. Brumhead, J. Lumin. **57**, 257 (1993).
[46]See http://hpc-education.unn.ru for Volga Research and Education Center for Supercomputing Technologies (last accessed March 01, 2017).
[47]V. Sadovnichy, A. Tikhonravov, Vl. Voevodin, and V. Opanasenko, "Lomonosov", *Supercomputing at Moscow State University. In Contemporary High Performance Computing: From Petascale toward Exascale (Chapman & Hall/CRC Computational Science)* (CRC Press, Boca Raton, LF, 2013), p. 283.